nature geoscience

ARTICLES

https://doi.org/10.1038/s41561-018-0064-1

Corrected: Publisher Correction

Modification of the Western Gondwana craton by plume–lithosphere interaction

Jiashun Hu[1], Lijun Liu[1]*, Manuele Faccenda[2], Quan Zhou[1], Karen M. Fischer[3], Stephen Marshak[1] and Craig Lundstrom[1]

The longevity of cratons is generally attributed to persistence of neutrally-to-positively buoyant and mechanically strong lithosphere that shields the cratonic crust from underlying mantle dynamics. Here we show that large portions of the cratonic lithosphere in South America and Africa, however, experienced significant modification during and since the Mesozoic era, as demonstrated by widespread Cretaceous uplift and volcanism, present-day high topography, thin crust, and the presence of seismically fast but neutrally buoyant upper-mantle anomalies. We suggest that these observations reflect a permanent increase in lithospheric buoyancy due to plume-triggered delamination of deep lithospheric roots during the Late Cretaceous and early Cenozoic periods. Lithosphere in these regions has been thermally reestablished since then, as confirmed by its present-day low heat flow, high seismic velocities and realigned seismic anisotropy. We conclude that the original lowermost cratonic lithosphere is compositionally denser than the asthenospheric mantle and can be removed when perturbed by underlying mantle upwelling. Therefore, it is the buoyancy of the upper lithosphere that perpetuates stabilization of cratons.

The stability and persistence of cratons (the long-lived, relatively stable portions of continents) has been a focus of sustained research for the past four decades. According to the traditional isopycnicity hypothesis, cratonic mantle lithospheres are highly depleted due to extensive melt extraction[1–4], which results in a highly viscous and neutrally to positively buoyant thermal boundary layer that persists for billions of years. This model, although elegant, does not readily explain apparent temporal variations in cratons, including significant elevation changes over time and episodic destruction of the deep lithosphere[3,4]. Recent measurements of seismic anisotropy suggest that the upper portion (<100–150 km depth) of the cratonic lithosphere has a seismic fabric that differs from the lithosphere below[5–7]. This new lithospheric structure is consistent with models that assume a compositionally stratified thermal boundary layer whose shallower depths are more depleted[8,9]. Such models spark questions about the buoyancy and stability of the cratonic lithosphere[2–4], especially as regards the relative contribution to density from composition and temperature at different depths[8–10]. Consequently, questions concerning how cratons can remain "stable" over billions of years and how they respond to dynamic processes in the underlying asthenosphere, still await an answer.

Here we investigate the density structure and temporal evolution of the cratonic lithosphere using diverse observational constraints, including topographic evolution, gravity anomalies, seismic tomography and anisotropy, tectonic reconstructions, and mantle flow. To avoid potential effects of Mesozoic–Cenozoic subduction on craton evolution[2,11,12], we focus on cratons bordering the South Atlantic passive margins (Fig. 1). This study area includes Precambrian regions of South America and Africa hosting cratons and Neoproterozoic orogens[13], regions that were once part of western Gondwana. A prominent feature of these continents is the widespread high (1 km or more) surface topography inside or on the edges of the São Francisco (SF), Congo (CG) and Kalahari (KH) cratons (Fig. 1a). Elevation of these regions is in sharp contrast to that of other cratons such as the West African (WA), Amazonian (AZ) and North American (NA) cratons that mostly display low topography[14,15].

Subsequently, we will address several key aspects related to the topographic evolution of the study area. First, most high topography in the region is isostatically supported by sub-crustal lithospheric mantle (Fig. 2). Second, this high topography developed during and since the late Mesozoic (Fig. 1b), as indicated by the presence of earlier marine-lacustrine depositional environments[16,17] and of widespread Cretaceous volcanic eruptions[18,19] and associated surface uplift[20–22] in these regions. Third, the upper mantle beneath the study area contains anomalous zones that have high seismic velocity but are close to being neutrally buoyant (Fig. 3), a feature characteristic of delaminated lithospheric mantle of cratons. Fourth, seismic anisotropy of lower cratonic lithosphere below these regions shows realignment to directions of the Cenozoic mantle flow (Fig. 4). Taken together, our analyses indicate that the western Gondwana cratonic lithosphere was modified through delamination beginning in the late Mesozoic, due to its interaction with mantle plumes.

Origin of high cratonic topography

Recent seismic studies[23–27] suggest that crustal thickness below significant portions of the high-topography regions (the SF and KH cratons and the periphery of the CG craton) is notably thinner than the surrounding continental regions (Supplementary Fig. 1a), probably in response to extensive Mesozoic surface erosion[18–22]. This relatively thin crust cannot compensate high topography, and thus must reflect positive buoyancy from the underlying mantle. Since high topography occurs within only part of the CG craton (Fig. 1a), density differences between cratonic and non-cratonic crust also cannot explain the observed topographic variation.

To gain further insight into the cause of topographic variation, we estimated the lithospheric residual topography by removing contributions of the crust (Supplementary Fig. 2a) and the sub-lithospheric mantle (Supplementary Fig. 3a), neither of which can explain the high surface topography (see Supplementary Materials).

[1]Department of Geology, University of Illinois at Urbana-Champaign, Champaign, IL, USA. [2]Department of Geoscience, University of Padova, Padova, Italy. [3]Earth, Environmental, and Planetary Sciences, Brown University, Providence, RI, USA. *e-mail: ljliu@illinois.edu

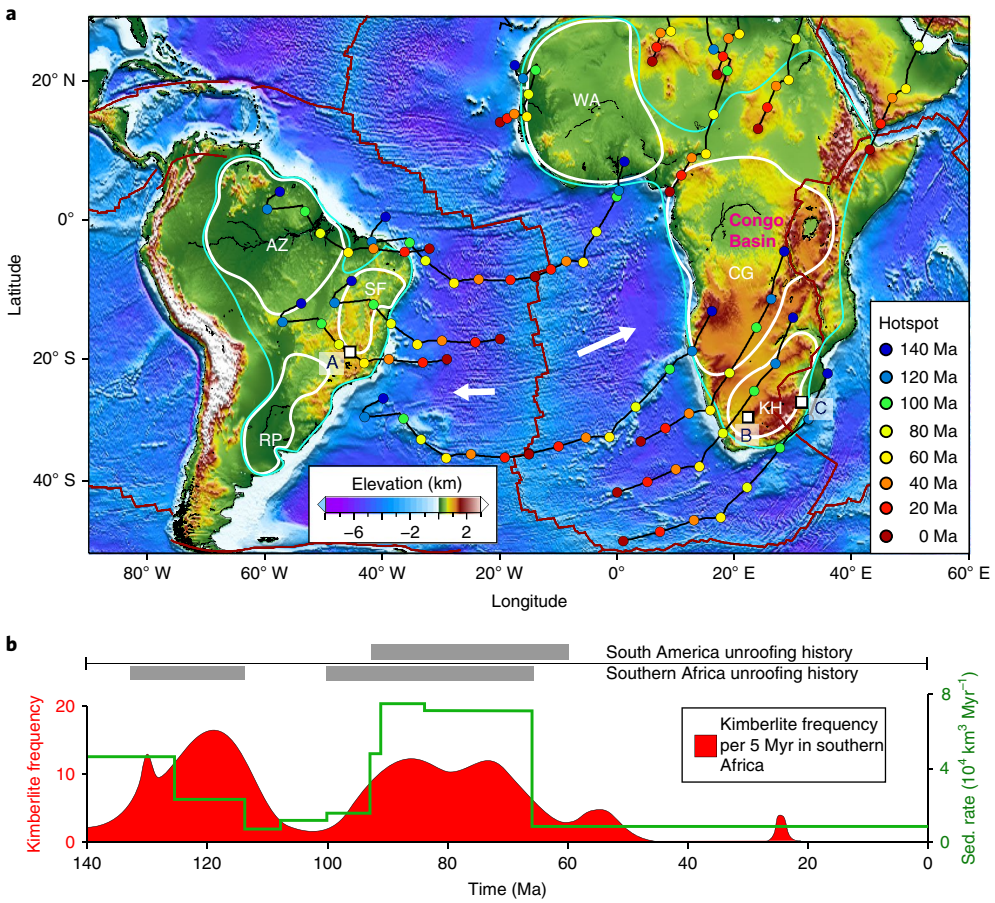

Fig. 1 | Topography and tectonic history of the South Atlantic margins. a, Anomalously high elevations in the KH, CG and SF cratons. In contrast, AZ, RP and WA cratons display low topography. White and cyan contours outline major cratons and Precambrian shields[13]. Coloured dots and black lines are reconstructed hotspot tracks. Thick white arrows indicate average Cenozoic plate motion directions. White squares (A–C) are several Cretaceous volcanic eruptions[19,21]. **b**, Kimberlite (red region) ages in southern Africa[57], accumulative sedimentation rate (green line) along the southern African coast[39], and unroofing history (thick grey bars) of the high-topography cratons (CG, KH and SF)[20–22].

In addition to the lack of correlation of crustal thickness with topography discussed above, recent geodynamic studies reveal neutral-to-negative dynamic topography in our study region[28–30], a result confirmed by our calculations using recent tomography images[31,32] (Supplementary Fig. 4). Consequently, the resulting lithospheric residual topography displays a peak-to-trough variation of up to 2 km (Fig. 2a), with positive areas correlating with the prominent high land-surface topography (Fig. 1). Most high residual topography occurs inside the cratons, with only a minor portion over the Neoproterozoic (Brasiliano or Pan African) orogens (Fig. 2a). This result suggests that high cratonic topography, in regions of thin crust, reflects lithospheric buoyancy heterogeneities. A similar analysis of the gravity field further supports this conclusion, with negative lithospheric gravity anomalies in high-topography regions (Fig. 2b).

To evaluate whether inferred lithospheric buoyancy heterogeneity is thermal or compositional in origin, we examined seismic, heat-flow, and xenolith data. The presence of high shear velocities[31–36] (Fig. 3, Supplementary Figs. 5,6), low attenuation[37] and cold geotherms inferred from heat flow[38] beneath both high-topography regions of KH, CG and SF and the two low-topography cratons of WA and AZ (Fig. 3, Supplementary Figs. 5,6) indicates that cold lithosphere extends down to depths of >200 km (refs [34,37]). Lithosphere thermal thicknesses inferred from shear velocities[34] vary by <25 km among the KH, CG, SF, WA and AZ cratons. Also, residual topography (Fig. 2a) does not correlate consistently with regional variations in thermal buoyancy of the mantle inferred from attenuation[37], either within or between cratons. Lithosphere thermal thickness inferred from heat flow[38] varies by <100 km, with high-topography cratons being slightly thinner (Supplementary Fig. 7). Lithospheric temperature estimates from mantle xenoliths also reveal similar to slightly higher (by <150 K) temperature beneath the KH craton compared to intact cratons such as the Slave[4]. Taking an upper limit (150 K) of these inferred temperature variations within the lower 100 km of the lithosphere, the associated thermal buoyancy could account for <500 metres of topography, in sharp contrast to the much larger variation (up to 2 km) of lithospheric residual topography (Fig. 2). Thus, we conclude that a significant fraction of the apparent lithospheric buoyancy reflects composition.

Cretaceous uplift due to lithospheric delamination

To better understand the origin of high-topography cratons, we also evaluated their temporal evolution. The SF craton has gained >1 km of surface elevation since the Cretaceous, relative to the adjacent AZ craton[16]. As a result, Late Jurassic–Early Cretaceous shallow-marine to lacustrine sedimentary strata in eastern Brazil now lie well above sea level[16]. Most of the uplift probably occurred during the Late Cretaceous in association with >3 km of denudation in eastern Brazil (Fig. 1b); the greatest denudation occurred along the northeastern edge of AZ[16] and over the entire SF[20,21], regions that presently have positive residual topography (Fig. 2a). Similarly, southern Africa—a region that had undergone subsidence during the Jurassic (as indicated by occurrence of sedimentary deposits of this age[17])—

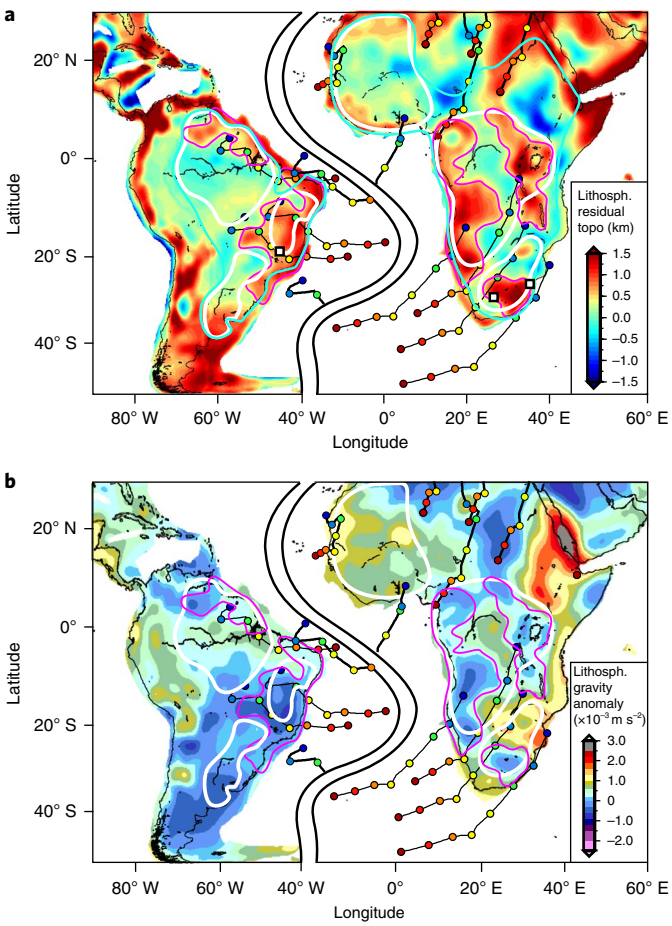

Fig. 2 | Lithospheric residual topography and gravity. a, Residual topography corrected for both Airy compensation of crustal effect and sub-lithospheric dynamic topography (Supplementary Fig. 3a). Magenta contours outline the regions with positive residual topography, implying the spatial extent of delamination. Note the association of positive residual topography with cratons. **b**, Residual gravity anomaly obtained by removing crustal, topographic, and sub-lithospheric contributions (Supplementary Fig. 3b) from free-air gravity (refer to Methods for details). Other notations are the same as those in Fig. 1.

experienced rapid uplift and denudation during the Cretaceous (Fig. 1b), as revealed by analysis of kimberlite diatremes[19], by thermochronology studies of the KH[22], and by evaluation of sedimentation history along the southern African coast[39].

Dynamic topography due to sub-lithospheric convection is unlikely to have caused the Cretaceous uplift and present high residual topography (Fig. 2a), for two reasons. First, recent estimates on changes in dynamic topography due to mantle convection since 100 Myr ago (Ma) reveal subsidence, not uplift, in eastern South America[28,29]. Similarly, little Cenozoic dynamic uplift took place in southern Africa[29,30]. Second, observed residual topography in our study area has a wavelength of <500 km (Fig. 2), while dynamic topography usually occurs over a wavelength of >1,000 km (Supplementary Fig. 4).

Since dynamic topography cannot explain observed uplift, we also examined the role that lithosphere delamination may have served in increasing cratonic lithospheric buoyancy, for delamination can cause isostatic uplift. A rapid increase of heat flow during the Late Cretaceous in both South America and southern Africa[19,21], and the contemporaneous disappearance of high-pressure garnet-facies in South America[21], provide independent evidence that the lowermost lithosphere was removed. In addition, the temporal correlation (Fig. 1b) among the two-pulse history of kimberlite eruption with more fertile composition from the second phase[40], the circum-Africa sedimentation rate[39], and the unroofing history for the KH, further support regional modification of the southern African lithosphere[40].

In regions far from subduction zones, mantle upwelling in plumes represents the most likely candidate for triggering lithosphere delamination. By reconstructing the trajectory of southern Atlantic hotspots[41] back to the Early Cretaceous using a recent plate reconstruction[42] (Fig. 1), we find that Cretaceous-aged hotspot tracks coincide with regions of high topography in both South America and southern Africa (Figs. 1 and 2). An independent validation of this reconstruction comes from the match of hotspots with dated Late Cretaceous volcanism (white squares in Fig. 1) in both Brazil and South Africa. This correlation implies a potential causal relationship among these phenomena. The most intense Late Cretaceous kimberlitic volcanism in the SF and KH cratons occurred primarily along their edges (Fig. 1), possibly implying the location of initial lithosphere delamination. Thermochronology studies in southern Africa reveal a migration of exhumation from the edge to the interior of KH during 90–60 Ma[22], consistent with a progressive peeling off of cratonic lithosphere toward the centre.

Both warming of the lithosphere and delamination of high-density materials can result in local buoyancy increase and surface uplift. The coherently fast seismic velocities of the thick lithospheres[31–36] and low present-day surface heat flow[38] suggest that the thermal perturbation caused by the Cretaceous plume–lithosphere interaction has now largely disappeared (Fig. 3, Supplementary Fig. 5). This disappearance is consistent with the time required for a new thermal boundary layer to replace the delaminated lower lithosphere (Supplementary Fig. 8). Therefore, the present-day high topography must reflect a permanent loss of a compositionally dense layer of material from the original lithosphere.

Can the proposed delaminated lithosphere be detected within the present-day mantle? A three-dimensional representation of mantle seismic structure (Fig. 3) reveals multiple voluminous high-velocity anomalies within the sub-lithosphere mantle below the south Atlantic margins. These mantle structures seem to be well resolved, as they are similar among different tomography models (Supplementary Figs. 5, 6). Since these regions have not experienced subduction since the early Mesozoic[42], these anomalies cannot represent subducted slabs. Previously, they were interpreted as zones of cold downwelling along lithospheric margins, due to edge-driven convection[43]. We suggest instead that they represent the foundered segments of lithospheric mantle.

This concept is supported by a separate study in which we quantitatively evaluated the mantle flow associated with the subduction of the Nazca Plate relative to the other high-velocity anomalies in Fig. 3 by simultaneously matching mantle flow predictions to observations of surface-wave anisotropy and shear-wave splitting[44] (Supplementary Figs. 10,11). Fits to both regional and local anisotropy measurements require that the Nazca slab is the dominant cause of downwelling and that other high-velocity anomalies are mostly passively drifting and generating negligible vertical mantle flow (Fig. 3). This result requires the south Atlantic upper-mantle anomalies to be close to neutrally buoyant.

According to our subduction model[44], the mantle beneath an overriding plate, such as South America, undergoes pressure-gradient driven Poiseuille flow. In contrast, beneath plates not near a subduction zone, mantle undergoes plate-motion driven Couette flow (Fig. 3). Consequently, present-day mantle structure further supports the lithosphere delamination hypothesis in that the geometry and location of these high-velocity anomalies (Fig. 3) are best explained as foundered lithosphere fragments left behind as South America and Africa moved apart since the Cretaceous (Fig. 3,

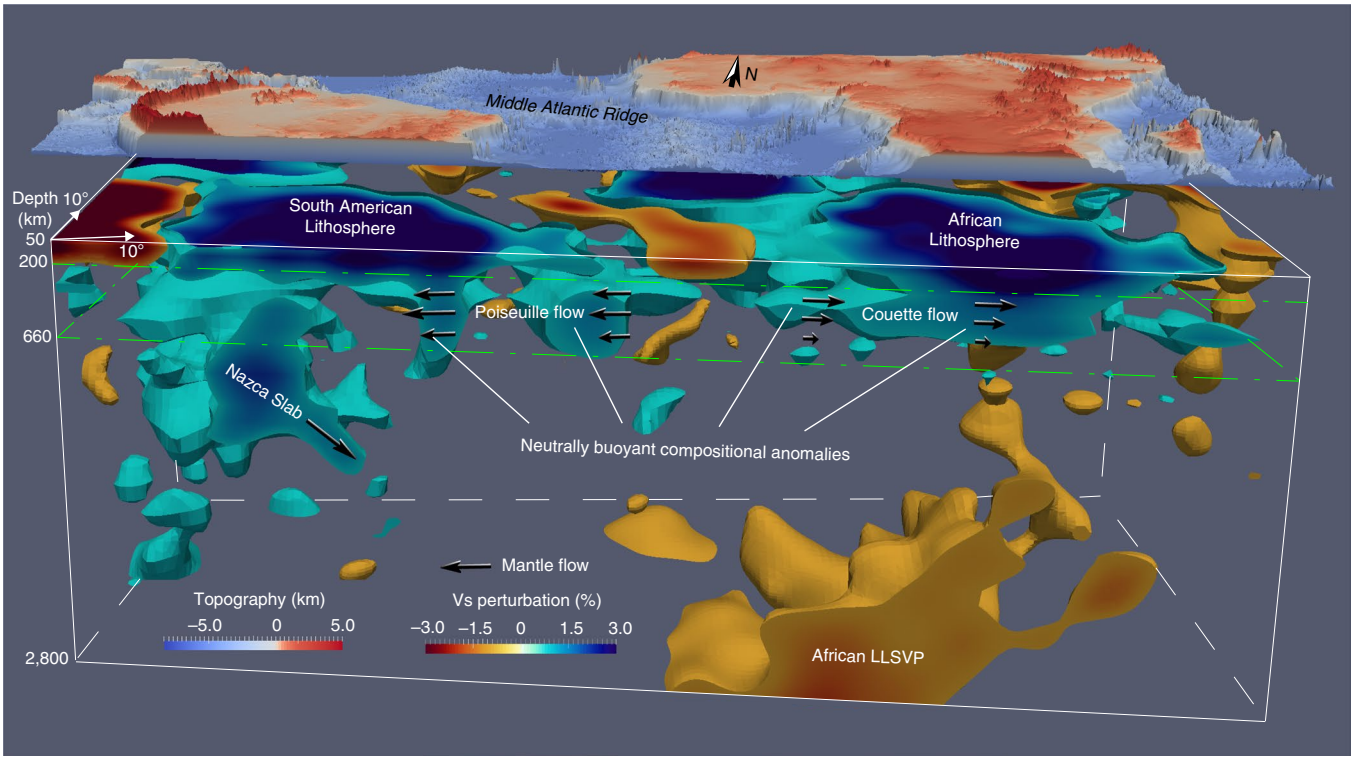

Fig. 3 | Seismic structure of the lithosphere and underlying mantle in the study region. The 3D visualization is based on the S40RTS tomography model[32], with the volume of fast structure showing anomalies at > 0.8%, and that for slow structure at < −1.0%. The colours on top highlight the topography contrasts. Black arrows indicate Cenozoic mantle flow, and interpretations of various high-velocity mantle structures are inferred from our geodynamic modelling of seismic anisotropy[44]. Note the overall westward drift of the upper mantle beneath the South American plate driven by Nazca subduction. LLSVP, large low-shear wave velocity province.

Supplementary Figs. 5, 6). The tendency for the delaminated materials to remain on the South American side of the Atlantic may reflect the stronger westward upper-mantle Poiseuille flow drawn by the down-going Nazca slab[44] (Fig. 3).

Cenozoic realignment of lithospheric seismic anisotropy

Lithospheric mantle that has undergone shear during the Cenozoic should display seismic anisotropy similar to that of recent asthenosphere flow. Comparison of azimuthal anisotropy[6] with that predicted by Cenozoic mantle flow, as a function of depth (see Supplementary Materials), therefore, can provide another important test of our model[44]. Robust anisotropy predictions within the asthenosphere below continental South America and surrounding oceans (Supplementary Figs. 10,11) allow us to apply the modelling results to the interior of the cratonic lithosphere.

Lack of correlation between the observed anisotropy in the uppermost mantle (<100 km) with that of the asthenosphere below suggest that fabrics at this depth are mostly 'fossil' signals (Fig. 4a,e), meaning relicts of pre-Cenozoic shear. At depths of ≥100 km, the correlation clearly improves in most non-cratonic regions (Fig. 4), consistent with their thin lithospheres (Fig. 3) and increasing influence of Cenozoic shear. The East African Rift region does not display anisotropy compatible with Cenozoic shear at >150 km depth (Fig. 4g, h), probably because of perturbations by upper-mantle upwelling (Fig. 3, Supplementary Fig. 2). In contrast, correlation of anisotropy is poor below the low-topography cratons, which are inferred to have intact mantle lithospheres (AZ and WA). This lack of correlation emphasizes that mantle deformation did not take place within the intact cratonic lithosphere during the Cenozoic[5,6].

However, in most high-topography cratonic regions, observed anisotropy aligns with predicted mantle shear at depths as shallow as 100 km, such as in SF (Fig. 4). A similar correlation of observed and predicted anisotropy results when a different anisotropy model[45] is employed (Supplementary Fig. 12a,c). This obvious regional realignment of lower lithosphere anisotropy with Cenozoic mantle flow in regions of Mesozoic modification suggests that the lithospheric fabrics of these cratons were reset. Another recent anisotropy model[46] confirms this conclusion for depths of <150 km, but displays significant discrepancy at greater depths (Supplementary Fig. 12b,d). Since this model fails to match our well-predicted asthenospheric deformation, and probably the shear-wave splitting observations over South America[44] as well (Supplementary Fig. 12), we suggest that the other two anisotropy models[6,45] better represent lowermost lithosphere fabrics in our study region.

Mechanically, fabric resetting could be due to either local deformation of the original lithosphere[11] or growth of a new thermal boundary layer after delamination (Fig. 5). We suggest a combination of both mechanisms. On the one hand, the isostatic uplift of topography requires removal of dense lithospheric materials. On the other hand, the observed high-velocity (>2%) lithosphere at 200 km and below (Fig. 3, Supplementary Fig. 5) requires compositional (for example, garnet or MORB, Supplementary Fig. 9) in addition to thermal effects (Supplementary Fig. 8). Therefore, we propose that delamination happened mostly within the lowermost cratonic lithosphere where high-density materials exist, and that lithosphere below ~100 km was not necessarily removed entirely but instead underwent shear sufficient to realign its crystallographic anisotropy with that of the ambient mantle. This concept can be further verified by examining the spatial extent of anisotropy realignment, where the realigned area in Africa is much larger than the zones of high residual topography (Fig. 2), with the former also closely correlating with the province of Cretaceous kimberlites[47] (Supplementary Fig. 13).

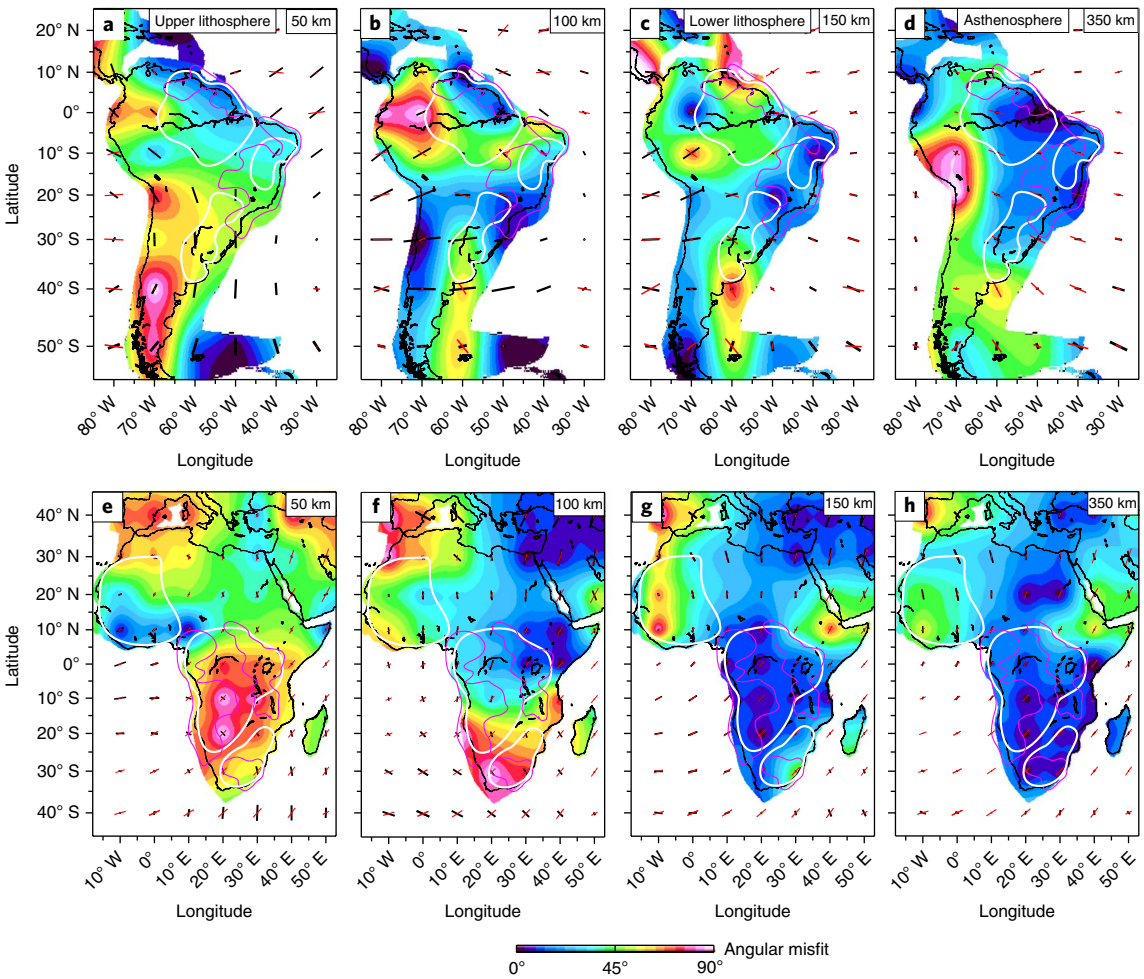

Fig. 4 | Comparison of observed and mantle-flow-induced seismic anisotropy. a–d, Azimuthal anisotropy at different depths beneath South America. Black bars are observations from YB12sv[6], and red bars are predictions[44]. The background colour represents the angular misfit between the two. The 350 km depth represents the asthenosphere. Note the increasing fit of anisotropy with depth in regions where deep lithosphere delamination (magenta contours) is inferred, implying Cenozoic shearing of these parts of the craton lithosphere. **e–h**, Same as **a–d**, but for Africa, where the comparison of observed and predicted anisotropy yields a similar conclusion. The poor fit in the northern East Africa Rift at depths > 100 km is probably due to active mantle upwelling that is not modelled in our anisotropy calculation.

Implications for density and evolution of cratonic lithosphere

In order for the lowermost cratonic lithosphere to delaminate, its density must be greater than that of the surrounding asthenosphere (Fig. 5a). Also, since present-day craton topography in our study area rises significantly higher than the pre-delamination topography reflected in Cretaceous uplift and present positive residual topography, the delaminated lithosphere must also have been denser than the subsequently formed thermal boundary layer. This proposal also explains why 'intact cratons' (for example, WA and AZ) have lower topography than that of 'delaminated cratons' (for example, SF, CG and KH). More reasoning along this line is in the Methods section. Our proposal contrasts with the traditional view that cratonic roots have approximately neutral buoyancy at all depths[1,3,4]. We propose instead that the upper lithospheric mantle of cratons is highly depleted and chemically buoyant, perhaps even more so than has been yet inferred from mantle xenoliths[4,40]. In intact cratons, the lower lithospheric mantle is more fertile, and grades downwards into a purely thermal boundary layer, which contains zones or layers (>200 km in depth) enriched in high-density minerals (Fig. 5a).

Our model is consistent with the occurrence of garnet-peridotite in lower portions of intact cratons, such as Slave and pre-Cenozoic KH cratons[3,4,21,40], and with high seismic velocities in the average lowermost (150–250 km) cratonic lithosphere[35]. Assuming a 50-km thickness of this high-density layer, the residual topography and gravity (Fig. 2) require 20% excess garnet-peridotite relative to a neutrally buoyant lowermost lithosphere, if the density of garnet-peridotite is ~10% higher than that of peridotite[4]. We propose that this high-density layer may have been emplaced during craton formation[48] and/or represents secular accumulation of basaltic melts from the deep mantle[49].

Our lithosphere-density model also explains several enigmatic properties of the prominent upper-mantle high-velocity seismic anomalies below the south Atlantic (Fig. 3, Supplementary Fig. 5). These include the presence of such anomalies in regions far away from subduction zones. Notably, delaminated lithosphere consisting of both dense garnet-peridotite and buoyant harzburgite (Fig. 5b) should have small initial negative buoyancy whose magnitude would also decrease with depth as temperature increases. A delayed post-garnet transformation within the warming delaminated root at 660-km depth[50] would generate additional positive buoyancy and further prohibit penetration into the lower mantle. This concept explains, first, the stagnation of the delaminated materials at the base of the upper mantle (Figs. 3 and 5c), and, second, their minimal

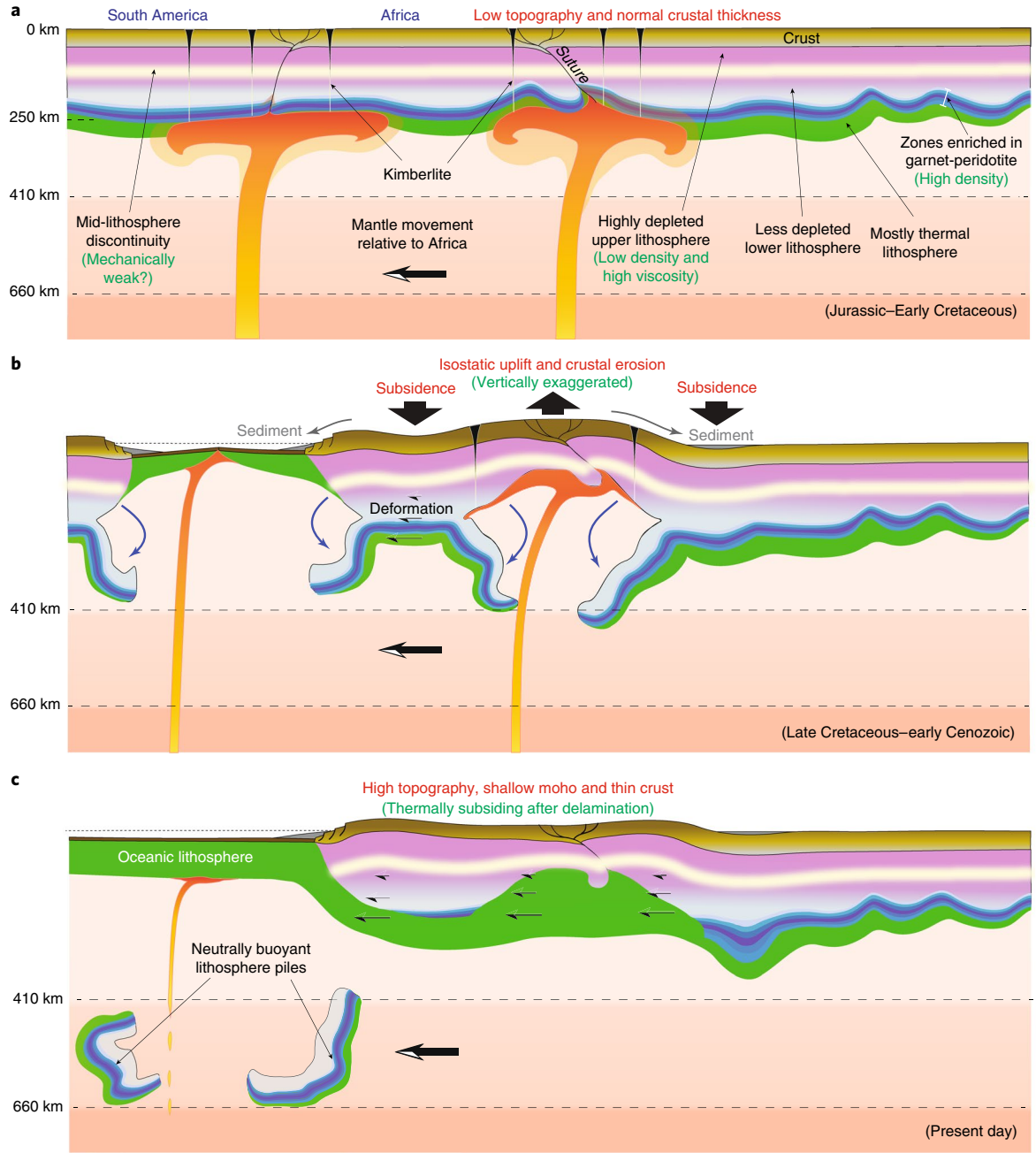

Fig. 5 | Schematic illustration of proposed cratonic lithosphere evolution since the Cretaceous. a, Sustained plume activity weakens the intact cratonic lithosphere by warming and metasomatism, forming kimberlites. **b**, Removal of deep mantle lithosphere including the garnet-peridotite layer and some harzburgite lithosphere. Both the surface and the Moho uplift isostatically, with erosion causing crustal thinning. **c**, Both internal shear of the lithosphere below the mid-lithosphere discontinuity and growth of a new thermal boundary in regions of delamination record recent mantle deformation with seismic anisotropy. The foundered lithosphere segments stagnate above the lower mantle due to their overall neutral buoyancy. Both high topography and shallow Moho reflect the lower density of the new thermal lithosphere compared to the intact lithosphere.

net buoyancy, thus avoiding generation of local convection as required by seismic anisotropy (Supplementary Figs. 10,11). Finally, the high seismic velocities of these anomalies (Fig. 3, Supplementary Fig. 5) are consistent with the enrichment of harzburgite and garnet at relatively low temperatures (Supplementary Fig. 9). We note that the minimum depth (~100 km) of anisotropy realignment broadly correlates with the mid-lithospheric discontinuities (MLDs) commonly found beneath continents[26,51–54]. This correlation implies that the MLD may represent a mechanically weak layer inside the lithosphere, below which shear deformation (>100 km) and ultimately delamination (>150–200 km) could occur more easily than in the lithosphere layer above. This conclusion is consistent with recent suggestions that the MLD represents the top of a weak layer of solidified volatile-rich melt accumulation[49,55]. Such a weak layer could serve as a decoupling surface between the upper and lower lithospheres during extension[56], and thereby could facilitate mobilization and delamination of dense deep lithosphere (Fig. 5).

Taken together, results presented in this paper indicate that lowermost cratonic mantle lithosphere may be episodically removed when sufficiently perturbed by mantle processes (Fig. 5b), while the depleted buoyant lithosphere tends to remain stable so that its crust maintains cratonic characteristics through geological time

(Fig. 5c). Figure 5 emphasizes the key features of cratonic lithosphere destabilization, during which deformation and removal of the dense root facilitates kimberlite volcanism[18–22], isostatic surface uplift (Figs. 1 and 2a), and shallow Moho and thin crust (Supplementary Fig. 1a). We further propose that zones where lower lithosphere was removed take tens of millions of years to recover thermally, but the density of the new thermal root would remain less than that of the intact root. Indeed, cratons lacking Phanerozoic hotspot activity and nearby subduction, such as those in the Northern Hemisphere, have not undergone delamination since the Mesozoic and therefore display negative residual topography (Supplementary Fig. 14a) and positive mantle gravity anomalies (Supplementary Fig. 14b) in contrast to cratons affected by subduction, such as those in East Asia[11] and western North America[12], and cratons affected by mantle plumes, such as those in the Southern Hemisphere (Supplementary Fig. 13).

Methods

Methods, including statements of data availability and any associated accession codes and references, are available at https://doi.org/10.1038/s41561-018-0064-1.

Received: 14 June 2017; Accepted: 11 January 2018;
Published online: 19 February 2018

References

1. Jordan, T. H. Composition and development of the continental tectosphere. *Nature* **274**, 544–548 (1978).
2. Durrheim, R. J. & Mooney, W. D. Evolution of the precambrian lithosphere: seismological and geochemical constraints. *J. Geophys. Res.* **99**, 15359–15374 (1994).
3. Carlson, R. W., Pearson, D. G. & James, D. E. Physical, chemical, and chronological characteristics of continental mantle. *Rev. Geophys*. **43**, RG1001 (2005).
4. Lee, C.-T. A., Luffi, P. & Chin, E. J. Building and destroying continental mantle. *Annu. Rev. Earth Planet. Sci.* **39**, 59–90 (2011).
5. Yuan, H. & Romanowicz, B. Lithospheric layering in the North American craton. *Nature* **466**, 1063–1069 (2010).
6. Yuan, K. & Beghein, C. Seismic anisotropy changes across upper mantle phase transitions. *Earth. Planet. Sci. Lett.* **374**, 132–144 (2013).
7. Debayle, E. & Kennett, B. L. N. The Australian continental upper mantle: structure and deformation inferred from surface waves. *J. Geophys. Res. Solid Earth* **105**, 25423–25450 (2000).
8. King, S. D. Archean cratons and mantle dynamics. *Earth Planet. Sci. Lett.* **234**, 1–14 (2005).
9. Eaton, D. W. & Perry, H. K. C. Ephemeral isopycnicity of cratonic mantle keels. *Nat. Geosci.* **6**, 967–970 (2013).
10. Kaban, M. K., Mooney, W. D. & Petrunin, A. G. Cratonic root beneath North America shifted by basal drag from the convecting mantle. *Nat. Geosci.* **8**, 797–800 (2015).
11. Griffin, W. L., Andi, Z., O'Reilly, S. Y. & Ryan, C. G. Phanerozoic evolution of the lithosphere beneath the Sino-Korean Craton. *Mantle Dyn. Plate Interact. East Asia* **27**, 107–126 (1998).
12. Levander, A et al. Continuing Colorado plateau uplift by delamination-style convective lithospheric downwelling. *Nature* **472**, 461–465 (2011).
13. Alkmim, F. F. et al. Kinematic evolution of the Araçuaí–West Congo orogen in Brazil and Africa: nutcracker tectonics during the Neoproterozoic assembly of Gondwana. *Precam. Res.* **149**, 43–64 (2006).
14. Kaban, M. K., Schwintzer, P., Artemieva, I. M. & Mooney, W. D. Density of the continental roots: compositional and thermal contributions. *Earth Planet. Sci. Lett.* **209**, 53–69 (2003).
15. Mooney, W. D. & Kaban, M. K. The North American upper mantle: density, composition, and evolution. *J. Geophys. Res.* **115**, B12424 (2010).
16. Arai, M. Chapadas: relict of mid-Cretaceous interior seas in Brazil. *Rev. Bras. Geoci.* **30**, 436–438 (2000).
17. Catuneanu, O. et al. The Karoo basins of south-central Africa. *J. Afr. Earth Sci.* **3**, 211–253 (2005).
18. Harman, R., Gallagher, K., Brown, R., Raza, A. & Bizzi, L. Accelerated denudation and tectonic/geomorphic reactivation of the cratons of northeastern Brazil during the Late Cretaceous. *J. Geophys. Res.* **103**, 27091–27105 (1998).
19. Hanson, E. K. et al. Cretaceous erosion in central South Africa: Evidence from upper-crustal xenoliths in kimberlite diatremes. *South Afr. J. Geol.* **112**, 125–140 (2009).
20. Cogné, N., Gallagher, K. & Cobbold, P. R. Post-rift reactivation of the onshore margin of southeast Brazil: evidence from apatite (U–Th)/He and fission-track data. *Earth Planet. Sci. Lett.* **309**, 118–130 (2011).
21. Read, G. et al. Stratigraphic relations, kimberlite emplacement and lithospheric thermal evolution, Quiricó Basin, Minas Gerais State, Brazil. *Lithos* **77**, 803–818 (2004).
22. Stanley, J. R., Flowers, R. M. & Bell, D. R. Kimberlite (U–Th)/He dating links surface erosion with lithospheric heating, thinning, and metasomatism in the southern African Plateau. *Geology* **41**, 1243–1246 (2013).
23. Laske, G., Masters, G., Ma, Z. & Pasyanos, M. Update on CRUST1.0 - A 1-degree Global Model of Earth's Crust. *Geophys. Res. Abstr.* **15**, EGU2013–2658 (2013).
24. Reid, A. B., Ebbing, J. & Webb, S. J. Comment on 'A crustal thickness map of Africa derived from a global gravity field model using Euler deconvolution' by Getachew E. Tedla, M. van der Meijde, A. A. Nyblade and F. D. van der Meer. *Geophys. J. Int.* **189**, 1217–1222 (2012).
25. Assumpção, M., Feng, M., Tassara, A. & Julià, J. Models of crustal thickness for South America from seismic refraction, receiver functions and surface wave tomography. *Tectonophysics* **609**, 82–96 (2013).
26. Liu, L., K. Liu and S. Gao. Lithospheric layering beneath southern Africa constrained by S-to-P receiver functions. In AGU Fall General Assembly 2016. abstr. DI51A-2660 (American Geophysical Union, 2016).
27. Globig, J. et al New insights into the crust and lithospheric mantle structure of Africa from elevation, geoid, and thermal analysis. *J. Geophys. Res. Solid Earth* **121**, 5389–5424 (2016).
28. Shephard, G. E., Müller, R. D., Liu, L. & Gurnis, M. Miocene drainage reversal of the Amazon River driven by plate-mantle interaction. *Nat. Geosci.* **3**, 870–875 (2010).
29. Flament, N., Gurnis, M. & Müller, R. D. A review of observations and models of dynamic topography. *Lithosphere* **5**, 189–210 (2012).
30. Moucha, R. & Forte, A. M. Changes in African topography driven by mantle convection. *Nat. Geosci.* **4**, 707–712 (2011).
31. French, S., Lekic, V. & Romanowicz, B. Waveform tomography reveals channeled flow at the base of the oceanic asthenosphere. *Science* **342**, 227–230 (2013).
32. Ritsema, J., Deuss, A., van Heijst, H. J. & Woodhouse, J. H. S40RTS: a degree-40 shear-velocity model for the mantle from new Rayleigh wave dispersion, teleseismic traveltime and normal-mode splitting function measurements. *Geophys. J. Int.* **184**, 1223–1236 (2011).
33. Pasyanos, M. E., Masters, T. G., Laske, G. & Ma, Z. LITHO1.0: an updated crust and lithospheric model of the Earth. *J. Geophys. Res.* **119**, 2153–2173 (2014).
34. Priestley, K. & McKenzie, D. The relationship between shear wave velocity, temperature, attenuation and viscosity in the shallow part of the mantle. *Earth Planet. Sci. Lett.* **381**, 78–91 (2013).
35. Adams, A. & Nyblade, A. Shear wave velocity structure of the southern African upper mantle with implications for the uplift of southern Africa. *Geophys. J. Int.* **186**, 808–824 (2011).
36. Feng, M., Assumpção, M. & Van der Lee, S. Group velocity tomography and lithospheric S-velocity structure of the South American continent. *Phys. Earth Planet. Inter.* **147**, 315–331 (2007).
37. Dalton, C. A., Bao, X. & Ma, Z. The thermal structure of cratonic lithosphere from global Rayleigh wave attenuation. *Earth Planet. Sci. Lett.* **457**, 250–262 (2017).
38. Artemieva, I. Global 1 degrees x 1 degrees thermal model TC1 for the continental lithosphere: Implications for lithosphere secular evolution. *Tectonophysics* **416**, 245–277 (2006).
39. Guillocheau, F. et al. Quantification and causes of the terrigeneous sediment budget at the scale of a continental margin: a new method applied to the Namibia–South Africa margin. *Basin Res.* **24**, 3–30 (2012).
40. Griffin, W. L. et al. The origin and evolution of Archean lithospheric mantle. *Precambrian Res.* **127**, 19–41 (2003).
41. Courtillot, V., Davaille, A., Besse, J. & Stock, J. Three distinct types of hotspots in the Earth's mantle. *Earth Planet. Sci. Lett.* **205**, 295–308 (2003).
42. Müller, R. D. et al. Ocean basin evolution and global-scale plate reorganization events since Pangaea breakup. *Annu. Rev. Earth Planet. Sci.* **44**, 107–138 (2016).
43. King, S. & Ritsema, J. African hot spot volcanism: small-scale convection in the upper mantle beneath cratons. *Science* **290**, 1137–1140 (2000).
44. Hu, J., Faccenda, M. & Liu, L. Subduction-controlled mantle flow and seismic anisotropy in South America. *Earth Planet. Sci. Lett.* **470**, 13–24 (2017).
45. Schaeffer, A. J., Lebedev, S. & Becker, T. W. Azimuthal seismic anisotropy in the Earth's upper mantle and the thickness of tectonic plates. *Geophys. J. Int.* **207**, 901–933 (2016).
46. Debayle, E., F. Dubuffet, and S. Durand, An automatically updated S-wave model of the upper mantle and the depth extent of azimuthal anisotropy. *Geophys. Res. Lett.* **43**, 674–682, (2016).
47. Yaxley, G. M. et al. The discovery of kimberlites in Antarctica extends the vast Gondwanan Cretaceous province. *Nat. Commun.* **4**, 2921 (2013).

48. Walter, M. J. Melting of garnet peridotite and the origin of komatiite and depleted lithosphere. *J. Petrol.* **39**, 29–60 (1998).
49. Rader, E. et al. Characterization and petrological constraints of the midlithospheric discontinuity. *Geochem. Geophys. Geosys.* **16**, 3484–3504 (2015).
50. Stixrude, L. & Lithgow-Bertelloni, C. Thermodynamics of mantle minerals-II. Phase equilibria. *Geophys. J. Int.* **184**, 1180–1213 (2011).
51. Wittlinger, G. & Farra, V. Converted waves reveal a thick and layered tectosphere beneath the Kalahari super-craton. *Earth Planet. Sci. Lett.* **254**, 404–415 (2007).
52. Sodoudi, F. et al. Seismic evidence for stratification in composition and anisotropic fabric within the thick lithosphere of Kalahari Craton. *Geochem. Geophys. Geosys.* **14**, 5393–5412 (2013).
53. Selway, K., Ford, H. & Kelemen, P. The seismic mid-lithosphere discontinuity. *Earth Planet. Sci. Lett.* **414**, 45–57 (2015).
54. Fischer, Karen M., Ford, Heather A., Abt, David L., Rychert, Catherine A. The Lithosphere–Asthenosphere boundary. *Ann. Rev. Earth Planet. Sci.* **38** 551–575, (2010).
55. Chen, L. et al. Presence of an intralithospheric discontinuity in the central and western North China Craton: Implications for destruction of the craton. *Geology* **42**, 223–226 (2014).
56. Liao, J., Gerya, T. & Wang, Q. Layered structure of the lithospheric mantle changes dynamics of craton extension. *Geophys. Res. Lett.* **40**, 5861–5866 (2013).
57. Jelsma, H., Barnett, W., Richards, S. & Lister, G. Tectonic setting of kimberlites. *Lithos* **112S**, 155–165 (2009).

Acknowledgements

We thank T. Jordan, W. Mooney, S. Gao and L. Chen for helpful comments on the manuscript. L.L. acknowledges NSF grants EAR-1345135, 1554554, 1565640 and supercomputing allocation on Blue Waters through ACI-1516586. M.F. acknowledges the grant Progetto di Ateneo FACCPTRAT12 from Università di Padova.

Author contributions

J.H. and L.L. conceived the project and performed the analysis. M.F. contributed to anisotropy and mineral physics. Q.Z., K.F., S.M. and C.L. contributed to gravity, seismology, geology and petrology, respectively. All authors participated in manuscript preparation.

Competing interests

The authors declare no competing financial interests.

Additional information

Supplementary information is available for this paper at https://doi.org/10.1038/s41561-018-0064-1.

Reprints and permissions information is available at www.nature.com/reprints.

Correspondence and requests for materials should be addressed to L.L.

Publisher's note: Springer Nature remains neutral with regard to jurisdictional claims in published maps and institutional affiliations.

Methods

Calculating mantle and lithosphere residual topographies. We first calculate the mantle residual topography by removing the Airy isostatic topography from the observed topography assuming an average crustal density of 2.8×10^3 kg m^{-3}. Since Crust1.0 model[23] (Fig. 1a) and other seismic studies[24–27] demonstrate similar regional-scale crust thickness variations, we use the former to estimate mantle residual topography. We also find that using the spatially varying crustal density from Crust1.0 does not change the pattern of residual topography. Geographically, the resulting positive mantle residual topography of up to 1.5 km (Fig. 2a) correlates closely with the prominent high surface topography (Fig. 1a), confirming its mantle origin. However, these residual topography signals have a wavelength of 200–500 km, precluding a lower mantle origin that suggests a wavelength of >1000 km. This observation is further consistent with recent understanding that the prominent large low-shear wave velocity provinces (LLSVP) in the lowermost mantle are compositionally distinct from the ambient mantle[58–60] and probably possess a neutral net buoyancy, leading to little dynamic uplift at the surface[29,30,61,62].

To isolate the topographic contributions from the lithosphere and sub-lithosphere mantle, we further estimate the convection-induced mantle dynamic topography with a global instantaneous model that has a lateral resolution of ~25 km and a variable vertical resolution that reaches a maximum of 5.5 km on the top. Here we define dynamic topography as due to sub-lithospheric (>300 km depth) mantle convection. We first converted seismic velocity perturbations to effective density anomalies using an empirical scaling[30,63], and adopted a radial mantle viscosity profile consistent with our forward subduction modelling[44]. Estimated dynamic topographies using the tomography models SEMum2[31] and S40RTS[32] are similar over South America and Africa, and we use the former in the final calculation since it is a more recent tomography model. The resulting dynamic topography (Supplementary Fig. 3a) is very similar to published models[29,30,61,62]. Our calculations suggest small-amplitude (<250 m), long-wavelength (>2,000 km) dynamic topography in most of the positive-residual-topography regions, implying little contribution. One exception is the Eastern African Rift (EAR), where prominent dynamic uplift is due to localized sub-lithospheric hot upwelling below the region[30].

We then estimated the residual topography associated with lithosphere buoyancy (Fig. 2a) by removing the topographic effect due to sub-lithospheric convection (Supplementary Fig. 3a) from the net mantle residual topography (Supplementary Fig. 2a). Thus estimated lithospheric residual topography within the craton regions (Fig. 2a) remains nearly identical to the net mantle residual tomography (Supplementary Fig. 2a). This is due to the lack of upper-mantle positive buoyancy, especially that associated with slow seismic anomalies, below these regions (Fig. 3, Supplementary Fig. 5). In this case, the lower-mantle large low-shear wave velocity province (LLSVP; Fig. 3) does not affect the prominent but localized positive residual topography whose wavelength is <500 km (Fig. 2a), because the LLSVP mostly affects the topography at a much larger wavelength (>1,000 km) and with a smaller amplitude (<300 m) (Supplementary Fig. 3a). Therefore, the high cratonic topography with elevated Moho should reflect mostly lithospheric buoyancy heterogeneities.

Mantle and lithospheric gravity anomalies. Gravity anomalies[64] provide another important constraint on lithosphere density structure. We first derived the mantle gravity anomaly (Supplementary Fig. 2b) by removing both the topographic and crustal effects from the free-air gravity anomaly (Supplementary Fig. 1b). We adopt the same approach as in earlier studies[14,15] using the Crust1.0 model[23] to calculate the gravity of the crust. Using a constant crustal density or the density structure provided in Crust1.0 leads to similar results. For the map shown in Fig. 2, we corrected the crustal effect with the Bouguer slab formula for different layers, while the density and the thickness of the layers are taken from Crust1.0. We find that the locations of the prominent negative (as low as -2×10^{-3} m s^{-2}) mantle gravity anomalies (Supplementary Fig. 2b) match almost exactly with those of mantle residual topography (Supplementary Fig. 2b). Since all topographic effects are removed from the mantle gravity calculation, its correlation with residual topography strongly supports the existence of low-density mantle underneath these regions, especially at lithospheric depths[15].

To quantify the lithospheric contribution to the gravity anomaly, we further removed the effects associated with the sub-lithospheric mantle density structure and that due to the dynamic topography of the core–mantle boundary (CMB). When calculating the sub-lithospheric mantle gravity, we assume a spherical Earth that is discretized by 16.8 million tesseroids with a size of $1°\times1°\times10$ km. The same mantle density and viscosity profile are used as that employed in estimating mantle dynamic topography. We found that the gravity effect of CMB topography cancels much of the LLSVP density effect, and that the resulting sub-lithospheric gravity anomaly (Supplementary Fig. 3b) is mostly affected by upper mantle buoyancy, especially the localized sub-lithospheric hot mantle beneath northeast Africa (Fig. 3a, Supplementary Fig. 5). Encouragingly, the inferred lithospheric gravity anomaly map (Fig. 2b) highlights the prominent negative gravity features associated with the high residual topography (Fig. 2a), almost all of which fall in cratonic regions. Consequently, these results reinforce the existence of local buoyancy heterogeneities within the cratonic lithosphere.

Modelling mantle flow and seismic anisotropy in South America and Africa. The plate velocities of South America and Africa have remained largely unchanged since 60 Ma (Fig. 1), implying a relatively stable mantle shear direction. Therefore, we approximate mantle-flow-induced anisotropy beneath Africa using the relative motion between the lithosphere and the deep mantle. However, mantle flow below South America has also been influenced by Cenozoic subduction of the Nazca plate, causing a deviation of flow from the absolute plate motion of South America[44]. Therefore, we designed a geodynamic model that reproduces the Nazca subduction history since 100 Ma and used the resulting mantle flow history to compute anisotropy below South America[44].

To quantitatively estimate the Cenozoic mantle flow and the resulting lattice preferred orientation of mantle minerals, we simulate the subduction history surrounding the South American continent since 100 Ma. The numerical model is centered on South American continent and covers a $100°\times100°\times2{,}900$ km physical domain in the EW × NS × vertical directions, respectively, to best represent the mantle dynamics. We adopt a forward model using a sequential data assimilation technique, such that the past subduction history is consistent with the reconstructed plate motions and seafloor age from ref. [42], and that resulting present-day slab structure satisfies that inferred seismically (Benioff zones in the upper mantle and seismic tomography in the lower mantle). A simultaneous match of all these observational data results in a tightly constrained history of mantle flow, as well as thermal and viscosity profiles of the geodynamic model. More details of the model set-up and mantle flow analysis can be found in ref. [44]. Thus predicted mantle flow beneath South America differs significantly from the direction of its absolute plate motion, indicating the dominant role of the subducting Nazca slab along the west coast and the secondary effects from slabs in the north[44].

Subsequently, we utilized the resulting Cenozoic mantle flow to calculate the present-day seismic anisotropy below South America. We assumed an initial mantle condition with randomly oriented olivine crystals, and then advected these crystals through the mantle flow to the present. The resulting anisotropy is mostly sensitive to the flow during the past 60 million years[44]. In order to evaluate the relationship between the observed surface wave anisotropy at lithosphere depths with that predicted from the mantle flow, we systematically vary the geometry and thickness of the South American cratons. We found that the best-fit model requires thick (>200 km) AZ and RP cratons to match the observed anisotropy that is both low-amplitude and mis-aligned with the mantle flow. However, in order to predict the large-amplitude and flow-parallel anisotropy beneath southeast Brazil, the model requires a thin (<100 km) SF craton and its surrounding continent. Although we did not model the thermal growth of the SF craton during the Cenozoic due to the limited numerical resolution of the large-scale model, the implication from the temporal development of seismic anisotropy suggests that the cratonic root must be largely absent during the early Cenozoic and that subsequent growth of the root should have had the same anisotropy signature as presented in Fig. 4.

The above approach of approximating seismic anisotropy is further confirmed by the data assimilation model: beneath an overriding plate such as the South American plate, mantle flow is controlled more by the slab-induced Poiseuille flow, and that beneath a non-overriding plate is dominated by plate-motion-controlled Couette flow (Fig. 3). This means we can estimate the overall anisotropy pattern using the surface plate motion in regions far away from subduction zones, such as Africa.

Discussion about lithosphere density and delamination. Here we provide more discussions about the logic of lithosphere structure and evolution.

First, the compositionally denser lowermost lithospheric layer is inferred by comparing Cretaceous uplift (several kms) and present high topography of the delaminated craton (without the original dense layer) to that of intact cratons (with the original dense layer). This observation suggests that the buoyancy of the cratonic lithosphere after delamination increases relative to pre-delamination, even after the full thermal recovery, as it has now. This increase cannot be due to upper lithosphere modification, since most changes in the depleted lithosphere should decrease, instead of increase, its buoyancy. Therefore, the best candidate for the buoyancy change is through the loss of original high-density material that most likely resides at the bottom of the lithosphere. In fact, the great depth of this layer (>200 km, see Fig. 5), together with its tendency to sink instead of rise, may have been inadequately sampled by xenoliths, which usually come from a depth range of <200 km. Seismological images clearly show that most cratonic lithosphere extends to below 200 km, providing room for this layer to exist. In cratons that have experienced shearing or delamination in the lower lithosphere, the re-stabilized or regrown thermal boundary would be cooler than but not necessarily chemically distinct from the asthenosphere. However, the negative thermal buoyancy of this lowermost lithosphere would be partially offset by the compositional buoyancy of the shallower cratonic mantle, enabling the persistence of the observed high residual topography (Figs. 2a and 5c). This new model implies a greater density stratification than that already inferred from mantle xenoliths that sample the lithosphere down to ~200 km depth[4,39].

Second, we suggest that xenolith data actually support our inferred lithosphere structure. As many earlier studies show, the extent of lithosphere depletion (through measuring Mg #) decreases with depth. Meanwhile, more high-density minerals,

such as garnet, occur in the lower portion of the cratonic lithosphere, so the lowermost cratonic lithosphere could be compositionally denser than the ambient mantle, if enough garnet is present. In fact, some earlier studies already imply a similar lithosphere structure as we present in this study. For example, Table 1 in ref. [65] showed the mineral abundances of peridotites from the southeast Slave Craton. The percentage of garnet in coarse garnet peridotite and deformed garnet peridotite can reach up to 10%, while that of garnet-rich wehrlites can reach ~20%, which could significantly increase the density. From equilibrium pressure and temperature estimates, these mantle xenoliths represent a depth range of ~160–250 km in the Slave Craton (Fig. 8 in ref. [65]). Similarly, Griffin and O'Reilly (2007)[66] inferred an eclogite-enriched layer at the base of the depleted subcontinental lithospheric mantle from xenoliths and proposed that eclogites may make up at least 30% of the mantle in this layer. These are potentially consistent with our model, in which a garnet-enriched zone represents our inferred dense basal layer (Fig. 5). We realize, however, that a systematic study of the depth-distribution of iron depletion and garnet-enrichment from xenoliths is necessary in future research.

Finally, we suggest that several tectonic drivers should exist for delamination to take place. These include: long-lived mantle plumes such as those occurred since the Jurassic[47] must develop, in order to efficiently weaken the lower lithosphere by thermal softening and metasomatism[67]; additional density increase during metasomatism and plume impingement would enhance lower lithosphere instability; both the Precambrian Pan-African orogeny[13] and the Mesozoic opening of the Atlantic margins created internal weakness and lateral thickness variations in the lithosphere, favouring edge-driven convection[43] and delamination (Fig. 5). The coexistence of these preconditions could explain localized lithosphere removal and resulting high residual topography along the south Atlantic margins (Fig. 2a), as well as the more widespread realignment of lithospheric fabrics (Fig. 4).

Code availability. The original version of the CitcomS code used to simulate mantle convection can be accessed at www.geodynamics.org/cig/software/citcoms/. The code used to generate plate-motion data can be accessed at www.gplates.org. The code used to make the figures can be accessed at www.soest.hawaii.edu/gmt/ and www.paraview.org/.

Data availability. The tomography model SEMum2, the crustal model CRUST1.0 and the surface wave anisotropy model of ref. [46] can be accessed at www.ds.iris.edu/ds/products/emc/. The tomography model S40RTS can be downloaded at http://jritsema.earth.lsa.umich.edu//Research.html. The surface wave anisotropy model of refs [6] and [45] are available through the links http://faculty.epss.ucla.edu/~cbeghein/research/models-download/ and https://andrewjschaeffer.wordpress.com/tomography/sl2016sva/#ModelDownloads, respectively.

References

58. Masters, G., Laske, G., Bolton, H. & Dziewonski, A. in *Earth's Deep Interior: Mineral Physics and Tomography From the Atomic to the Global Scale* (eds Karato, S.-I., Forte, A., Liebermann, R., Masters, G. & Stixrude, L.) 63–87 (American Geophysical Union Monograph, 2000).
59. Ni, S., Tan, E., Gurnis, M. & Helmberger, D. Sharp sides to the African superplume. *Science* **296**, 1850–1852 (2002).
60. McNamara, A. & Zhong, S. Thermochemical structures beneath Africa and the Pacific Ocean. *Nature* **437**, 1136–1139 (2005).
61. Steinberger, B. Effects of latent heat release at phase boundaries on flow in the Earth's mantle, phase boundary topography and dynamic topography at the Earth's surface. *Phys. Earth Planet. Inter.* **164**, 2–20 (2007).
62. Conrad, C. P. & Husson, L. Influence of dynamic topography on sea level and its rate of change. *Lithosphere* **1**, 110–120 (2009).
63. Simmons, N. A., Forte, A. M. & Grand, S. P. Joint seismic, geodynamic and mineral physical constraints on three-dimensional mantle heterogeneity: implications for the relative importance of thermal versus compositional heterogeneity. *Geophys. J. Int.* **177**, 1284–1304 (2009).
64. Bonvalot, S. et al. *World Gravity Map: 1:50,000,000 Map* (International Gravimetric Bureau, 2012).
65. Kopylova, M. G. & Caro, G. Mantle xenoliths from the southeastern slave craton: evidence for chemical zonation in a thick, cold lithosphere. *J. Petrol.* **45**, 1045–1067 (2004).
66. Griffin, W. L. & O'Reilly, S. Y. in *Developments in Precambrian Geology* (eds Martin, R. H. S., van Kranendonk, J. & Vickie, C. B.) Ch. 8.2, 1013–1035 (Elsevier, 2007); https://doi.org/10.1016/S0166-2635(07)15082-9
67. Wang, H., J. van Hunen & D. G. Pearson. The thinning of subcontinental lithosphere: the roles of plume impact and metasomatic weakening. *Geochem. Geophys. Geosys.* **16**, 1156–1171 (2015).